Microelectronics Reliability 54 (2014) 778–784

Contents lists available at ScienceDirect

Microelectronics Reliability

journal homepage: www.elsevier.com/locate/microrel

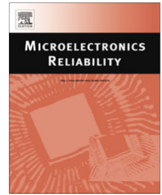

High performance of CNT-interconnects by the multi-layer structure

Wei-Chih Chiu *, Bing-Yue Tsui

Department of Electronics Engineering and Institute of Electronics, National Chiao Tung University, No. 1001 Ta-Hsueh Road, Hsinchu 30010, Taiwan, ROC

ARTICLE INFO

Article history:
Received 28 October 2013
Received in revised form 5 December 2013
Accepted 26 December 2013
Available online 24 January 2014

ABSTRACT

In this work, we propose two carbon nanotube (CNT) network fabrication processes, the normal spin rate coating (NR) and the slow spin rate coating (SR), and two interconnect structures, the single layer structure (SL) and the double layer structure (DL), to construct CNT-interconnects. We demonstrate and compare the performance of the CNT-interconnects with four kinds of process combinations: NR/SL, NR/DL, SR/SL and SR/DL. Generally, in the midst of these four combinations, the DL samples have higher conductive probabilities and less conductance variations, while SL/SR samples have the higher average conductance under the same amount of the CNT solution for CNT network formation. In addition, the phase transition phenomena occurred in the size dependent average conductance of CNT-interconnects are characterized and investigated by percolation theory. With the elongation of CNT-interconnects, the relationships between the average conductance and the square number would shift from linear region, power region to percolation region. Moreover, the results show that the resistance from the additional layer of Al_2O_3 in the double layer interconnect structure would influence the phase transition in the conductance of CNT-interconnects as well.

© 2013 Elsevier Ltd. All rights reserved.

1. Introduction

In the late 1990s, copper has been introduced into the integrated circuit manufacturing as an interconnect material of priority with the feature sizes decreasing [1]. However, with the continuous evolvement in the semiconductor technology, the available interconnect fabrication process has no longer been sufficient to keep abreast with the future CMOS technological generations. Constant scaling has been altering the electrical properties of copper, such as the conductivity and reliability, due to the additional electron–surface scattering, grain boundary scattering and surface roughness-induced scattering [2]. Besides, the fabrication processes for copper deposition, patterning and a more applicable barrier material to prevent the copper atoms from diffusing into the surrounding insulator have also become critical issues for the further development of the Cu-interconnects [3]. Therefore, new interconnect technology with high performance and easy fabrication processes has been greatly of concern for semiconductor industries.

The carbon nanotube (CNT), first discovered by Iijima in 1991 [4], has aroused plenty of interest owing to the extraordinary physical properties [5–7], such as high current density enduring ability (2.5×10^9 A/cm^2) and extremely high carrier mobility (2×10^4 cm^2/V s) [8], and has quickly been adopted for a variety of applications in these few years [9–11], particularly in the nanoelectronics area [12,13]. Although the tube-to-tube variations arising from non-idealities in the synthesis process have restricted the application of the CNTs [14], it has been proved that such issue could be effectively alleviated by the ensemble averaging over large amount of CNTs [15]. In spite of the fact that the unsatisfactory reliability still exists in CNT networks for now, but the nice performance and simple fabrication processes still make CNT networks viewed as one of the most efficacious approaches to integrating the CNTs into microelectronic fabrication.

Until now, several methods for the CNT network formation have constantly been proposed. For instance, spin coating the CNT solution directly onto a wafer [16], filtering out the solvent by vacuum filtration to deposit the CNTs on a substrate [17], transferring CNTs to a flexible plastic substrate by printing methods [18], or growing CNTs directly on dispersed catalysts by the CVD at temperatures higher than 400 °C [19]. Among these fabrication processes, the spin coating method possesses the merits of the most simplicity and being able to exercise in a low temperature process.

In early 2013, we adopted the slow rate spin coating (SR) and dry etching to fabricate CNT-interconnects in the single layer configuration (SL) and enhanced the maximum average sheet conductance to approximately 10^{-4} S by a total amount of 20 mL CNT solution [20]. However, due to the CNT synthesis process caused variations, it is difficult to narrow the conductance variations while simultaneously retain high conductive probabilities by such slow rate spin coating. Generally, it is found that, in most cases, the

* Corresponding author. Tel.: +886 6 2631802; fax: +886 3 5131570.
E-mail address: chiweich0327@gmail.com (W.-C. Chiu).

0026-2714/$ - see front matter © 2013 Elsevier Ltd. All rights reserved.
http://dx.doi.org/10.1016/j.microrel.2013.12.024

The Width Varying Series of CNT-Interconnects											
Length (L)	100 μm	100 μm	100 μm	100 μm	100 μm	100 μm	100 μm	100 μm	100 μm	100 μm	100 μm
Width (W)	500 μm	150 μm	100 μm	50 μm	25 μm	20 μm	17 μm	12 μm	10 μm	7 μm	5 μm
Square Number	0.2	0.7	1	2	4	5	6	8	10	15	20

The Length Varying Series of CNT-Interconnects											
Length (L)	5 μm	10 μm	25 μm	30 μm	40 μm	75 μm	100 μm	200 μm	300 μm	500 μm	1000 μm
Width (W)	5 μm	5 μm	5 μm	5 μm	5 μm	5 μm	5 μm	5 μm	5 μm	5 μm	5 μm
Square Number	1	2	5	6	8	15	20	40	60	100	200

Fig. 1. The CNT-interconnects fabricated by the SR/SL fabrication process with a total amount of 20 mL CNT solution. (a) Conductance statistics of the width varying series of CNT-interconnects. The inset is the specifications of the width varying series: 100 μm in lengths and a range from 500 μm to 5 μm in widths. (b) Conductance statistics of the length varying series of CNT-interconnects. The inset is the specifications of the length varying series: 5 μm in widths and a range from 5 μm to 1000 μm in lengths. The square numbers of a CNT-interconnect are determined by the length (*L*) divided by the width (*W*) of CNT-interconnects. (c) A top view schematic a set of four-probe bridge resistors for a CNT-interconnect conductance measurement. The spacing of 5 μm between two adjacent resistors is for precise interconnect conductance measurement.

conductance of the CNT-interconnects fabricated by 20 mL amount of the CNT solution has more than two orders of variations as shown in Fig. 1(a) and (b). Besides, the conductive probabilities of the long dimensional CNT-interconnects are quite low, such as 20% and 0% conductive probabilities of the CNT-interconnects with 100 and 200 square numbers, respectively, as demonstrated in Fig. 1(b). This present paper first demonstrates the performance of CNT-interconnects constructed by two kinds of spin coating methods, normal rate or slow rate spin coating, and then patterned by dry etching. Then, we will show that how the multi-layer interconnect structure improves the conductivity, the conductive probability and the conductance variation of CNT-interconnects. It is proved that the double layer interconnect structure is effective to reduce the conductance variations within almost one order, improve the conductive probabilities of the long dimensional CNT-interconnects and maintain the maximum average sheet conductance about 5×10^{-5} S at the same time. Finally, the phase transition phenomena in the size and the interconnect structure dependent CNT-interconnect electrical properties are included and investigated by percolation theory as well.

2. CNT-interconnect fabrication

In this experiment, we used "square number" as a unit, the length (*L*) divided by the width (*W*) of an interconnect, to characterize each CNT-interconnect dimension and sorted them into two series, the width varying series and the length varying series. In the width varying series, the lengths of CNT-interconnects are fixed at 100 μm and the widths range from 500 μm to 5 μm corresponding to 0.2–20 in square numbers. On the other hand, in the length varying series, the widths of CNT-interconnects are fixed at 5 μm and the lengths range from 5 μm to 1000 μm corresponding to 1–200 in square numbers. The detail geometries of the width and the length varying series of CNT-interconnects adopted for this work are listed in the insets of Fig. 1(a) and (b), respectively. Moreover, the precise gauge of individual CNT-interconnect conductance was done by a set of four-probe bridge resistors as depicted in Fig. 1(c).

To begin with, a boron-doped (100)-oriented 4-inch-diameter silicon wafer was first grown by a 200-nm-thick layer of thermal oxide and then capped with a 1-nm-thick layer of Al_2O_3 which was done by 250 cycles of atomic-layer deposition (ALD) with the precursors, trimethylaluminum (TAM) and water, in the temperature of 160 °C. The spin-coated CNT networks in our experiments were formed by the AP-grade discharge grown CNTs with the purity of 50–70% and residue catalysts of yttrium (Y) and nickel (Ni). These rod-like CNTs have an average diameter of 1.4 nm and an average length of 3.5 μm, and the ratio of the semiconducting and the metallic CNT distribution is approximately 2:1 as determined by the Raman spectroscopy [21].

The solution for CNT network formation was prepared by dissolving 2 mg CNT powder into dimethylformamide (DMF) solvent and then sonicating 24 h for uniform dispersion. There were two kinds of processes for the CNT network formation in this experiment, the normal rate spin coating (NR) and the slow rate spin coating (SR). The former process used a spin speed of 500 rpm for 30 s to coat the CNTs onto the wafer after 0.5 mL CNT solution was dropped by a dropper at the center per cycle, while the latter one lowered the spin speed to 100 rpm for 10 s per cycle [22]. In both cases, a heating process was utilized for evaporating the solvent out after each coating cycle. Then the sets of four-probe bridge resistors for conductance measurement were fabricated by depositing 60 nm Pd/Ti metal with the ratio about 9/1 by a co-sputtering technique and patterned by a lift off process. Finally, the CNT-interconnect construction was done by the O_2 plasma etching for single layer (SL) interconnect structure. Differing from the SL case, the double layer (DL) interconnect structure was built with an additional ALD made 1-nm-thick layer of Al_2O_3 deposited between two CNT networks as depicted in Fig. 2(a). After patterning the CNT-interconnects, the wafer was dipped into diluted HF solution for 5 s to remove the top Al_2O_3 layer outside the interconnect regimes before the O_2 plasma etching. The detail process flow for metal contact and interconnect of the DL samples formation is shown in Fig. 3.

In this work, we fabricated four kinds of CNT-interconnect samples for comparison and further optimization: NR/SL, NR/DL, SR/SL and SR/DL (The process for CNT network formation/ the interconnect structure). It is noted that, in the SL case, an amount of 20 mL (40 cycles) CNT solution in total was applied for the CNT network formation, while in the DL cases, the upper and bottom CNT networks were separately fabricated by 10 mL (20 cycles) CNT solution, as shown in Fig. 2(b).

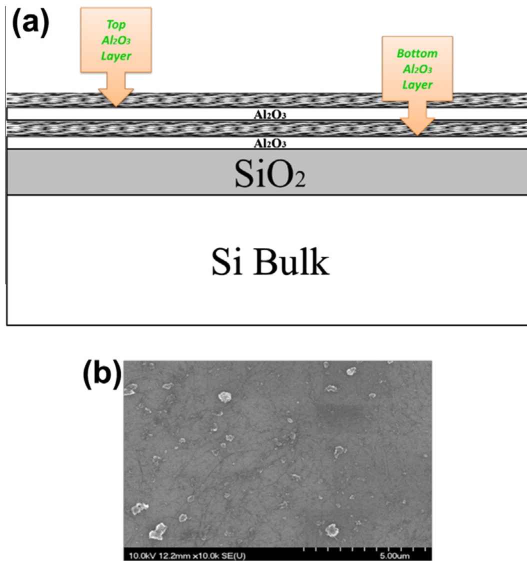

Fig. 2. (a) Schematic cross section of a CNT-interconnect in the double layer configuration. The top and bottom CNT networks are formed by the normal rate or the slow rate spin coating techniques with an amount of 10 mL CNT solution, respectively. (b) A SEM image of a CNT network fabricated by the slow rate spin coating with an amount of 20 mL CNT solution within an interconnect regime.

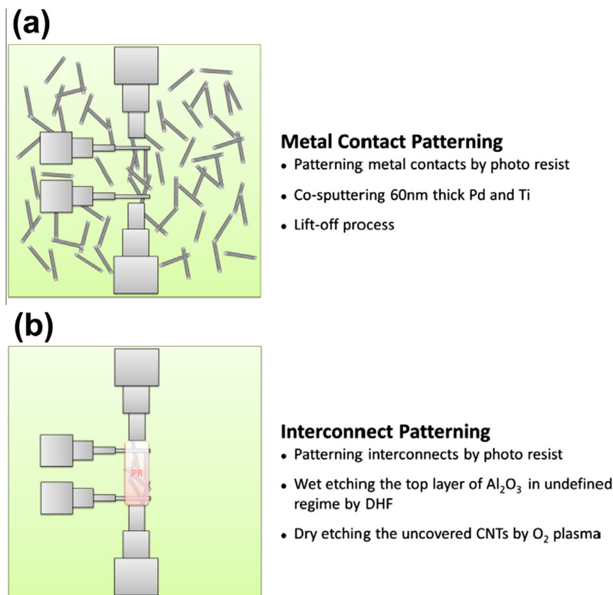

Fig. 3. A process flow for a double layer CNT-interconnect fabrication. (a) Four-probe bridge resistors formation. (b) CNT-interconnect formation.

3. Results and discussions

3.1. Characterizations of CNT-interconnects by the NR/SL and the NR/DL fabrication processes

Fig. 4 shows the conductance distribution and the histogram of the width varying NR/SL and NR/DL samples. In this study, the yield of CNT-interconnects was converted by the number of working interconnects in ten randomly selected samples for each conditions. The statistical distribution in Fig. 4 shows that the average sheet conductance of the NR/SL samples and the NR/DL samples ranges from 6.79×10^{-7} to 2.40×10^{-6} S and from 4.70×10^{-6} to 5.31×10^{-5} S, respectively. Generally, the NR/DL samples have

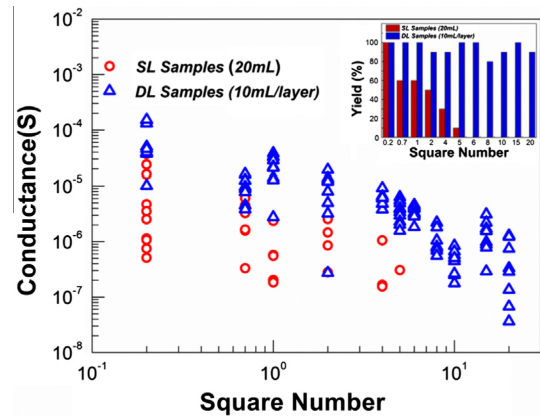

Fig. 4. Conductance statistics of the width varying series of CNT-interconnects built with the single layer (red) and the double layer (blue) interconnect structures and fabricated by a total amount of 20 mL CNT solution through the normal rate spin coating. The inset is the histogram of the number of working CNT-interconnects in the width varying series with the single layer (red) and the double layer (blue) interconnect structures fabricated by a total amount of 20 mL CNT solution through the normal rate spin coating. (For interpretation of the references to colour in this figure legend, the reader is referred to the web version of this article.)

higher conductance than that of the NR/SL samples under the same CNT-interconnect square numbers. In addition, in some cases, the conductance of the NR/DL samples gets more than one order enhanced. Moreover, the conductance variations in the NR/DL samples are almost within one order except for some CNT-interconnect samples with relatively long dimensions. In the inset of Fig. 4, all of the NR/DL samples have overwhelmingly higher conductive probabilities than those of the NR/SL samples. These results show that the double layer interconnect structure is able to greatly improve the performance of the CNT-interconnects with the normal spin rate coated CNT networks.

The reasons for such satisfactory results might mainly arise from the double layer interconnect structure. Past research has proved that the Al_2O_3 could uniformly distribute and attach the spin-coated CNTs on the wafer [23,24]. However, because of the finite stickiness from Al_2O_3 to CNTs, the deposited CNTs cannot unlimitedly accumulate with the increase of coating cycles. Therefore, some of coated CNTs would be thrown off the wafer during such fast spinning process which eventually results in poor performance of the CNT-interconnects in the single layer configuration. In the case of the DL samples, the top 1-nm-thick layer of Al_2O_3 might supply extra stickiness to capture more spin-coated CNTs onto the wafer which results in higher probabilities to form more percolative paths. Additionally, unlike the single layer interconnect structure, the electrons can only transport within single layer of a CNT network, while the electrons in the double layer interconnect structure can not only transmit via the tube-to-tube contact in the same layer of the CNT network [25] but also tunnel through the top Al_2O_3 layer to the other layer of the CNT network as depicted in Fig. 5. According to the research from Saraswat's group, the inserted 1-nm-thick Al_2O_3 layer does not form any resistance for electron tunneling [26]. In this way, it is more likely for CNT-interconnects to possess more CNT connected conductive paths and better electrical properties.

Fig. 6 shows the conductance distribution and the histogram of the length varying NR/SL and NR/DL samples. The statistical distribution in Fig. 6 shows that the average sheet conductance of the NR/SL samples and the NR/DL samples ranges from 5.71×10^{-6} to 9.98×10^{-6} and from 7.34×10^{-6} to 2.16×10^{-5}, respectively. In spite of the fact that the highest conductance values of the DL samples in some cases are slightly lower than those of the SL samples, but the DL samples basically have higher conductance and

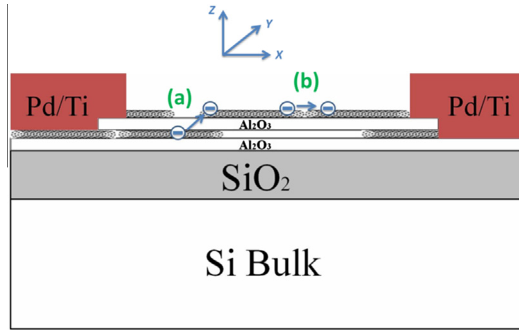

Fig. 5. Schematic electron transmission mechanisms of the CNT-interconnects with the double layer structure: (a) tunneling to the other layer of CNT network (b) tube-to-tube contact transfer in the same layer of CNT network.

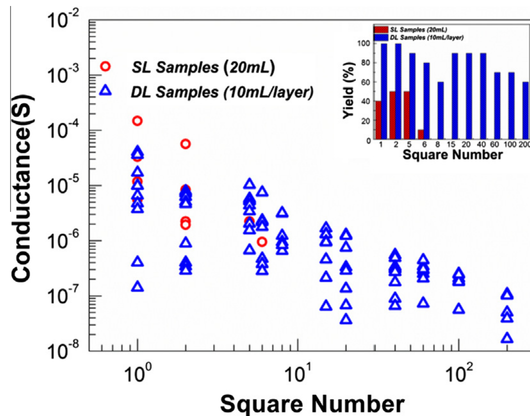

Fig. 6. Conductance statistics of the length varying series of CNT-interconnects built with the single layer (red) and the double layer (blue) interconnect structures and fabricated by a total amount of 20 mL CNT solution through the normal rate spin coating. The inset is the histogram of the number of working CNT-interconnects in the length varying series with the single layer (red) and the double layer (blue) interconnect structures fabricated by a total amount of 20 mL CNT solution through the normal rate spin coating. (For interpretation of the references to colour in this figure legend, the reader is referred to the web version of this article.)

more concentrated conductance distributions in most cases. However, the relatively larger than width varying CNT-interconnect conductance variations could be ascribed to the thin layer of Al_2O_3 inserted between the two CNT networks. In a CNT random network, the carrier transportation is dominated by the tube-to-tube Schottky emission [24], but the interconnects with the double layer structure has one more tunneling barrier from the top layer of Al_2O_3 apart from the resistance coming from the metallic/semi-conducting CNT interface [27]. Besides, compared with the width varying series of CNT-interconnects, the interconnect areas in length varying series are smaller, so that it is more difficult to accommodate sufficient CNTs and less likely for these limited number of the CNTs within the interconnect regime to link into conductive paths which eventually results in lower conductance and larger conductance variations of the DL samples.

However, it is worthy to note that the double layer structure renders the relatively high conductive probabilities to CNT-interconnects especially to the interconnects with a large number of square numbers, such as 70% in 100 square numbers and 60% in 200 square numbers as shown in the inset of Fig. 6. Such high conductive probabilities of the long dimensional CNT-interconnects might also attribute to the extra stickiness to CNTs and the uniformly distributing CNT ability from the top layer of Al_2O_3 in double layer structure.

3.2. Phase transitions in the size dependent conductivities of the NR/SL and the NR/DL CNT-interconnects

The conductive property of a large amount of randomly dispersing conductible and quasi one-dimensionally structural CNTs within a specified interconnect regime could be analyzed by the percolation theory [28,29] and expressed as follows [30]:

$$\sigma \propto (N - N_c)^{\alpha}, \tag{1}$$

where σ stands for the conductivity of a CNT-interconnect with the CNT density of N, and N_c is the critical CNT density. This is a threshold for the CNTs to connect into a least one conductive paths in a specific CNT cluster. The critical exponent, α is a space geometrically dependent parameter, and an exponent of 1.33 is theoretically for a conductive film in two dimensions while 1.94 in three dimensions. The critical density for the percolative model is given by

$$l\sqrt{\pi N_c} = 4.236, \tag{2}$$

where l is the average length of the CNTs. In 2004, the Grüner group used percolation theory to investigate the phase transition phenomena occurring in the CNT density dependent conductivities and distinguish the percolation region from the power region by the power fitting approach [30]. In 2013, we also took advantage of a similar method to prove that under a specified times of slow rate spin coating cycles for CNT-interconnect formation, varying the interconnect regime has a similar effect as the change of the CNT density and reasonably drew a conclusion about the equivalence of the CNT density with the reciprocal of the square number of CNT-interconnects. In addition, we also defined the critical square number to correspond to the critical density (percolation threshold) in the percolative relation. In this way, it is more legitimate to apply the percolation theory to the conductivities of the size varying CNT-interconnects [20]. Moreover, we further categorized the conductive characteristics of the CNT-interconnects into linear region, power region and percolation region with the increase of the CNT-interconnect square number [20]. However, differing from the SL CNT-interconnects, the DL interconnect structure builds CNT-interconnects into three dimensional conductive films. Therefore, it should be noticed that the power region of the DL samples is distinguished out by which the exponents of the fitting curve approaching or deviating 1.94 instead of 1.33.

Fig. 7 shows the fitting curves of average conductance of the width varying CNT-interconnects fabricated by the NR/SL and the NR/DL fabrication processes. By applying the power fitting approach, all sampling CNT-interconnects by the NR/SL fabrication process are sorted into percolation region because the exponents deviated from 1.33, when the fitting curve included less and less points excluding from the CNT-interconnects of $L \times W$ = 100 μm × 500 μm. On the other hand, the exponents of the fitting curve for the CNT-interconnects by the NR/DL fabrication process gradually closed to 1.94 after 100 μm × 5 μm, 100 μm × 7 μm, 100 μm × 10 μm, 100 μm × 12 μm, 100 μm × 17 μm and 100 μm × 20 μm interconnects were filtered out one by one which implies that these points are categorized into the percolation region, while the rest samples are around the power region. These results demonstrate that not only the interconnect size but also the interconnect structure would affect the characteristics of CNT-interconnects.

Fig. 8 shows the fitting curves of average conductance of the length varying CNT-interconnects fabricated by the NR/SL and the NR/DL fabrication processes. In this figure, all of the CNT-interconnects by the NR/SL fabrication process belongs to the percolation region also due to the deviation of the exponent from 1.33. In the length varying series of CNT-interconnects, owing to the smaller interconnect areas, the more influential resistance from

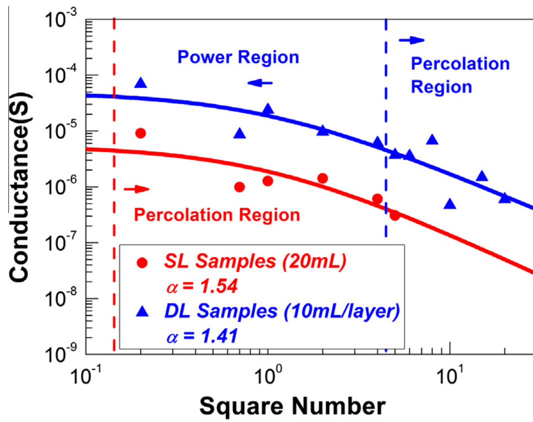

Fig. 7. Power functions of the average conductance versus the square number of the width varying CNT-interconnects with the single layer (red) or the double layer (blue) interconnect structures fabricated by a total amount of 20 mL CNT solution through the normal rate spin coating. In the width varying series, all SL samples are classified into the percolation region, while the DL samples with less than four square numbers belong to the power region and the rest CNT-interconnects are around the percolation region. (For interpretation of the references to colour in this figure legend, the reader is referred to the web version of this article.)

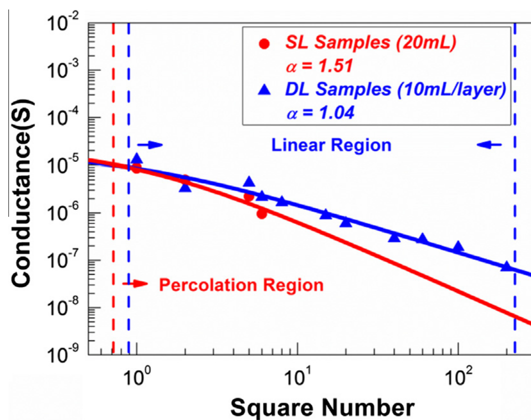

Fig. 8. Power functions of the average conductance versus the square number of the length varying CNT-interconnects with the single layer (red) or the double layer (blue) interconnect structures fabricated by a total amount of 20 mL CNT solution through the normal rate spin coating. In the length varying series, all SL samples are sorted into the percolation region while all DL samples proceeds to the linear region because of the resistance from the top layer of Al_2O_3 and mutual CNT contacts. (For interpretation of the references to colour in this figure legend, the reader is referred to the web version of this article.)

the extra layer of Al_2O_3 and resistance between CNTs bring about the linear related conductance with a critical exponent of 1.04 [31].

3.3. Characterizations of CNT-interconnects by the SR/SL and the SR/DL fabrication processes

Fig. 9 shows the conductance distribution and the histogram of the width varying SR/SL and SR/DL samples. The statistical distribution in Fig. 9 shows that the average sheet conductance of the SR/SL samples and the SR/DL samples ranges from 3.16×10^{-5} to 5.22×10^{-5} S and from 9.29×10^{-6} to 5.64×10^{-5} S, respectively. Compared with the CNT-interconnects fabricated by the normal rate spin coating process, the SR samples generally have higher conductance under the same square numbers of CNT-interconnects. It is believed that most of CNTs in solution during the slow rate spin coating process would be held on the substrate, so that the extra layer of Al_2O_3 in DL samples

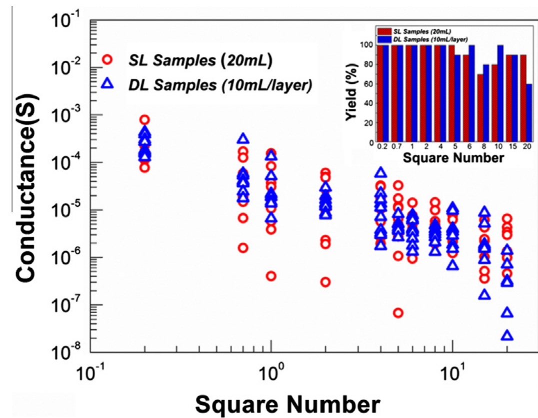

Fig. 9. Conductance statistics of the width varying series of CNT-interconnects built with the single layer (red) and the double layer (blue) interconnect structures and fabricated by a total amount of 20 mL CNT solution through the slow rate spin coating. The inset is the histogram of the number of working CNT-interconnects in the width varying series with the single layer (red) and the double layer (blue) interconnect structures fabricated by a total amount of 20 mL CNT solution through the slow rate spin coating. (For interpretation of the references to colour in this figure legend, the reader is referred to the web version of this article.)

demonstrates less superiority on the electrical performance than the case of the normal rate spin coating. Conversely, it becomes additional resistance to slightly lower the conductance of the DL samples. However, the weak Van der Waals forces between the CNTs causes some dispersed CNTs to bundle together before precipitation which leads in relatively higher conductance variations in the SL samples [32]. Therefore, it is concluded that the double layer structure could be effective to reduce the conductance variations. On the other hand, the inset of Fig. 9 shows that, in terms of the conductive probability, the performance of the SR/DL samples is competitive with that of the SR/SL samples. Both CNT-interconnect samples have above 60% of conductive probabilities under the same square numbers which verify that CNT-interconnects fabricated by the slow rate spin coating are likely to possess more CNT-linked conductive paths than those fabricated by the normal rate spin coating.

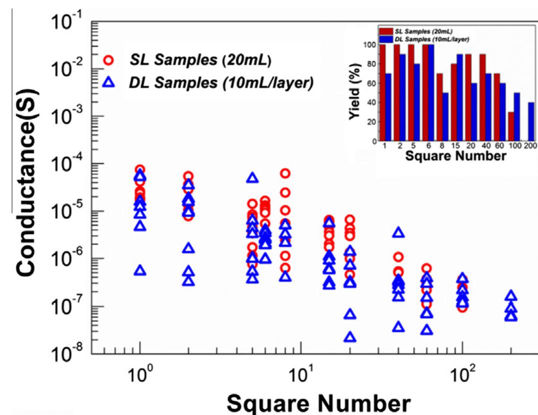

Fig. 10. Conductance statistics of the length varying series of CNT-interconnects built with the single layer (red) and the double layer (blue) interconnect structures and fabricated by a total amount of 20 mL CNT solution through the slow rate spin coating. The inset is the histogram of the number of working CNT-interconnects in the length varying series with the single layer (red) and the double layer (blue) interconnect structures fabricated by a total amount of 20 mL CNT solution through the slow rate spin coating. (For interpretation of the references to colour in this figure legend, the reader is referred to the web version of this article.)

Fig. 10 shows the conductance distribution and the histogram of the length varying SR/SL and SR/DL samples. The statistical distribution in Fig. 10 shows that the average sheet conductance of the SR/SL samples and the SR/DL samples ranges from 1.50×10^{-5} to 1.21×10^{-4} S and from 9.29×10^{-6} to 4.02×10^{-5} S, respectively. Like the case of the width varying CNT-interconnect case, most SL samples have higher conductance than that of the DL samples. However, in the length varying case, the conductance distribution of the DL samples seems more dispersed than those of the SL samples. The failure of the double layer structure might be ascribed to the top layer of Al_2O_3 between the two CNT networks as well. Because the slow rate spin-coated CNTs could be effectively kept on the wafer, the CNT density of the SL samples would be twice higher than that of each layer in the DL samples. Besides, the current conduction in the SL samples could be just directly via the tube-to-tube contact, but the electrons might need to continually tunnel through the top Al_2O_3 layer up and down to complete the whole transmission. Therefore, there is no apparent enhancement in the conductance values and distributions of the DL samples. Nonetheless, there are two points worth highlighting. One is that the range of the average sheet conductance of the width varying DL samples almost overlaps with that of the length varying DL samples fabricated by the normal rate or slow rate spin-coated CNT networks, and the CNT-interconnects with 100 and 200 square numbers have an average sheet conductance of about 1.94×10^{-5} S and 1.85×10^{-5} S with the conductive probabilities of 50% and 40%, respectively, as demonstrated in the inset of Fig. 10. These results once again show that the double layer structure could not only strengthen the stickiness to CNTs but also disperse the CNTs more uniformly on the wafer. In this way, it is likely for more CNTs to participate in the connection of conductive paths and make higher reliabilities of CNT-interconnects and higher conductive probabilities of the long dimensional CNT-interconnects.

3.4. Phase transitions in the size dependent conductivities of the SR/SL and the SR/DL CNT-interconnects

Fig. 11 shows the fitting curves of average conductance of the width varying CNT-interconnects fabricated by the SR/SL and the SR/DL fabrication processes. Because of the high CNT densities in the CNT-interconnects fabricated by the slow rate spin coating process, all of the SL and DL samples proceeds into power region and linear region also determined by the power fitting approach. The power region of the DL samples includes 100 μm × 25 μm, 100 μm × 20 μm, 100 μm × 17 μm, 100 μm × 12 μm, 100 μm × 10 μm, 100 μm × 7 μm and 100 μm × 5 μm with the exponent of 1.86.

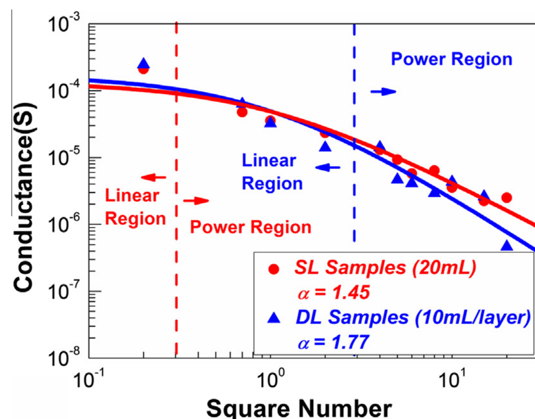

Fig. 11. Power functions of the average conductance versus the square number of the width varying CNT-interconnects with the single layer (red) or the double layer (blue) interconnect structures fabricated by a total amount of 20 mL CNT solution through the slow rate spin coating. In the width varying series, the SL sample with 0.2 square numbers and the DL samples with less two square numbers are classified into the linear region, while the rest SL and DL samples are around the power region. The larger linear region of the DL samples arises from the resistance from the top layer of Al_2O_3. (For interpretation of the references to colour in this figure legend, the reader is referred to the web version of this article.)

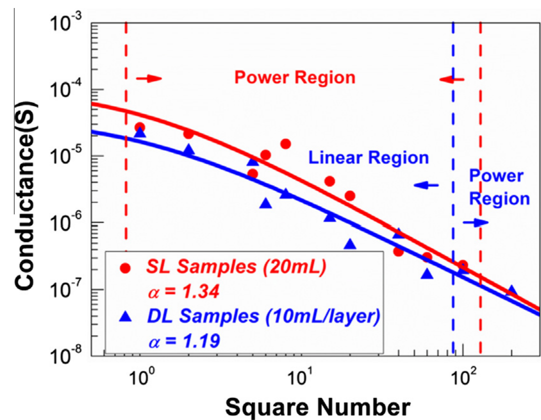

Fig. 12. Power functions of the average conductance versus the square number of the length varying CNT-interconnects with the single layer (red) or the double layer (blue) interconnect structures fabricated by a total amount of 20 mL CNT solution through the slow rate spin coating. In the length varying series, all SL samples locate at the power region, while the DL samples with less than 100 square numbers are around the linear region. (For interpretation of the references to colour in this figure legend, the reader is referred to the web version of this article.)

Fig. 12 shows the fitting curves of average conductance of the length varying CNT-interconnects fabricated by the SR/SL and the SR/DL fabrication processes. As we have shown, the shrinkage of the interconnect area would strengthen the influence of resistance from the interlayer of Al_2O_3 and the metallic/semiconducting CNT interfaces which leads to the enlargement of the linear region of the length varying DL samples.

4. Conclusions

In this work, we have fabricated the CNT-interconnects with two kinds of CNT network formation processes, the normal rate and the slow rate spin coating, and two kinds of interconnect structures, the single layer and the double layer interconnect structure, and demonstrated the performance of CNT-interconnects with four combinations of the processes. By the percolation theory, we illustrated the interconnect size, the structure and the processes for the CNT network formation dependent phase transition phenomena and classified into three regions based on the characterizations. In the case of the CNT networks formed by the normal rate spin coating, the DL samples generally shows better conductivity, narrower variations, better conductivity reliabilities and higher conductive probabilities. On the other hand, in the case of the CNT networks formed by the slow rate spin coating, even though the DL samples shows slightly worse conductivity but narrower variations, better conductivity reliabilities and higher probabilities especially for the CNT-interconnects with large square numbers still make the double layer interconnect structure very attractive. It should be noted that the smaller CNT-interconnect area, the larger the conductance variations of the DL samples would be. Finally, although the spin coating process and the multi-layer interconnect structure demonstrate some advantages to the CNT-interconnects, we cannot but admit that the conductivity of CNT-interconnects with multi-layer interconnect structure is still much lower than that of copper, 5.88×10^5 S/cm. However, the application of CNT-interconnects to flexible electronics and wearable electronics

is still very promising [33,34]. Therefore, in order to optimize the performance of CNT-interconnects with the multi-layer interconnect structure, the further work might concern with maximizing the conductance of each single layer of CNT networks (increasing the spin coating cycles), minimizing the resistance from the interlayer of Al_2O_3, or introducing more interlayer of Al_2O_3 into CNT-interconnects.

Acknowledgements

The authors would like to thank the Nano Facility Center of National Chiao-Tung University for providing the experimental facilities. This work was supported in part by the Ministry of Education in Taiwan under ATU Program, and was supported in part by the National Science Council, Taiwan, ROC under the contract No. NSC 100-2221-E-009- 010-MY2.

References

[1] Andricacos PC, Uzoh C, Dukovic JO, Horkans J, Deligianni H. Damascene copper electroplating for chip interconnections. IBM J 1998;42:567–74.
[2] Rossnagel SM, Kuan TS. Alteration of Cu conductivity in the size effect regime. J Vac Sci Technol 2004;B22:240–7.
[3] Andricacos PC. Copper on-chip interconnections, a breakthrough in electrodeposition to make better chips. Electrochem Soc Interface 1999:32–7.
[4] Iijima S. Helical microtubules of graphitic carbon. Nature 1991;354:56–8.
[5] Ebbesen TW, Lezec HJ, Hiura H, Bennett JW, Ghaemi HF, Thio T. Electrical conductivity of individual carbon nanotubes. Nature 1996;382:54–6.
[6] Lee RS, Kim HJ, Fischer JE, Thess A, Smalley RE. Conductivity enhancement in single-walled carbon nanotube bundles doped with K and Br. Nature 1997;388:255–7.
[7] Frank S, Poncharal Ph, Wang ZL, de Heer WA. Carbon nanotube quantum resistors. Science 1998;280:1744–6.
[8] Ebbesen TW, Lezec HJ, Hiura H, Bennett JW, Ghaemi HF, Thio T. Electrical conductivity of individual carbon nanotubes. Nature 1996;382:54–6.
[9] Tsukagoshi K, Alphenaar BW, Ago H. Coherent transport of electron spin in a ferromagnetically contacted carbon nanotube. Nature 1999;401:572–4.
[10] Son YW, Cohen ML, Louie SG. Half-metallic grapheme nanoribbons. Nature 2006;444:347–50.
[11] Misewich JA, Martel R, Avouris P, Tsang JC, Heinze S, Tersoff J. Electrically induced optical emission from a carbon nanotube FET. Science 2003;300:783–6.
[12] Avouris P, Chen Z, Perebeinos V. Carbon-based electronics. Nat Nanotechnol 2007;2:605–13.
[13] Cao Q, Rogers JA. Ultrathin films of single-walled carbon nanotubes for electronics and sensors: a review of fundamental and applied aspects. Adv Mater 2009;21:29–53.
[14] Tseng YC, Phoa K, Carlton D, Bokor J. Effect of diameter variation in a large set of carbon nanotube transistors. Nano Lett 2006;6:1364–8.
[15] Snow ES, Novak JP, Campbell PM, Park D. Random networks of carbon nanotubes as an electronic material. Appl Phys Lett 2003;82:2145–7.
[16] Kaempgen M, Duesberg GS, Roth S. Transparent carbon nanotube coatings. Appl Surface Sci 2005;252:425–9.
[17] Kymakis E, Amaratunga GAJ. Single-wall carbon nanotube/conguated polymer photovoltaic devices. Appl Phys Lett 2002;80:112–4.
[18] Hur SH, Park OO, Rogers JA. Extreme bendability of single-walled carbon nanotube network transferred from high-temperature growth substrates to plastic and their use in thin-film transistors. Appl Phys Lett 2005;86:243502.
[19] Kang SJ, Kocabas C, Ozel T, Shim M, Pimparkar N, Alam MA, et al. High-performance electronics using dense, perfectly aligned arrays of single-walled carbon nanotubes. Nature 2007;2:230–6.
[20] Chiu WC, Tsui BY. Characteristics of size dependent conductivity of the CNT-interconnects formed by low temperature process. Microelectron Reliab 2013;53:906–11.
[21] Dresselhaus MS, Jorio A, Souza Filho AG, Dresselhaus G, Saito R. Raman spectroscopy on one isolated carbon nanotube. Physica B 2002;323:15–20.
[22] Chiu WC, Tsui BY. Investigation into the performance of CNT-interconnects by spin coating technique. The 5th IEEE International nanoelectronics conference (INEC) January, 2013:240–1.
[23] Lee TC, Tsui BY, Tzeng PJ, Wang CC, Tsai MJ. An optimized process for high yield and high performance carbon nanotube field effect transistors. Microelectron Reliab 2010;50(5):666–9.
[24] Chang HY, Tsui BY. Low-temperature wafer-scale fabrication of carbon nanotube network thin-film transistors: geometry effect and transport mechanism. The 4th IEEE International nanoelectronics conference (INEC) Jan, 2011;B3-4:21–4.
[25] Kumar S, Murthy JY, Alam MA. Percolating conduction in finite nanotube networks. Phys. Rev. Lett. 2005;95:066802–5.
[26] Jason Lin J-Y, Roy Arunanshu M, Nainani Aneesh, Sun Yun, Saraswat Krishna C. Increase in current density for metal contacts to n-germanium by inserting TiO_2 interfacial layer to reduce Schottky barrier height. Appl Phys Lett 2011;98:092113.
[27] Fuhrer MS, Nygard J, Shih L, Forero M, Yoon Young-Gui, Mazzoni MSC, et al. Crossed nanotube junctions. Science 2000;288:494–7.
[28] Pike GE, Seager CH. Percolation and conductivity: a computer study. I Phys Rev 1974;10(B):1421–34.
[29] Seager CH, Pike GE. Percolation and conductivity: a computer study II. Phys Rev 1974;10(B):1435–46.
[30] Hu L, Hecht DS, Grüner G. Percolation in transparent and conducting carbon nanotube networks. Nano Lett 2004;4:2513–7.
[31] Wang Q, Dai J, Li W, Wei Z, Jiang J. The effects of CNT alignment on electrical conductivity and mechanical properties of SWNT/epoxy nanocomposites. Composite Sci Technol 2008;68:1644–8.
[32] Thess R, Lee P, Nikolaev HJ, Dai P, Petit J, Xu CH, et al. Crystalline ropes of metallic carbon nanotubes. Science 1996;273:483–7.
[33] Hur S-H, Park OO, Rogers JA. Extreme bendability of single-walled carbon nanotube networks transferred from high-temperature growth substrates to plastic and their use in thin-film transistors. Appl Phys Lett 2005;86:243502.
[34] Bradley K, Gabriel J-CP, Grüner G. Flexible nanotube electronics. Nano Lett 2003;3:1353–5.